Protein Capsules Assembled *via* Isobutyramide Grafts: Sequential Growth, Biofunctionalization, and Cellular Uptake

Damien Mertz,[†] Jiwei Cui,[†] Yan Yan,[†] Glyn Devlin,[‡] Christophe Chaubaroux,[§] Alexandre Dochter,[⊥] Roxane Alles,[¶] Philippe Lavalle,[§] Jean Claude Voegel,[§] Anton Blencowe,[†] Pascal Auffinger,[#] and Frank Caruso[†,*]

[†]Department of Chemical and Biomolecular Engineering, The University of Melbourne, Parkville, Victoria 3010, Australia, [‡]Australian Synchrotron, Clayton, Victoria 3168, Australia, [§]Institut National de la Santé et de la Recherche Médicale, INSERM Unité 977, Faculté de chirurgie dentaire, Université de Strasbourg, 67085 Strasbourg, France, [⊥]Centre National de la Recherche Scientifique, UPR22, Institut Charles Sadron, 23 rue du Loess, BP 84047, 67034 Strasbourg, France, [¶]Institut National de la Santé et de la Recherche Médicale, INSERM Unité 748, 3 rue Koeberlé, 67000 Strasbourg, France, and [#]Architecture et Réactivité de l'ARN, Université de Strasbourg, IBMC, CNRS, 15 rue René Descartes, 67084 Strasbourg, France

ABSTRACT We report the sequential assembly of proteins *via* the alternating physical adsorption of human serum albumin (HSA) and chemical grafting with isobutyramide (IBAM) or bromoisobutyramide (BrIBAM) groups. This approach, performed on silica template particles, leads to the formation of noncovalent protein films with controlled growth at the nanometer scale. Further, after template removal, hollow protein capsules with tunable wall thicknesses and high mechanical stability are obtained. The use of BrIBAM, compared to IBAM grafts, leads to significantly thicker capsule walls, highlighting the influence of the bromine atoms in the assembly process, which is discussed in terms of a theoretical model of noncovalent interactions. Another feature of the process is the possibility to functionalize the HSA capsules with other biologically active macromolecules, including enzymes, polysaccharides, or DNA plasmids, demonstrating the versatility of this approach. We also report that BrIBAM-HSA and IBAM-HSA capsules display negligible cytotoxicity *in vitro* with HeLa cells and that their cellular uptake is dependent on the thickness of the capsule walls. These findings support the potential use of these protein capsules in tailored biological applications such as drug delivery.

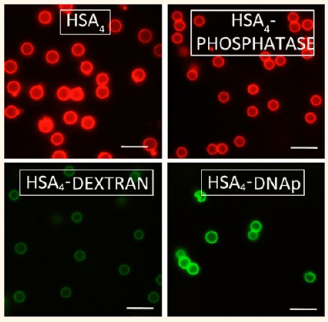

KEYWORDS: protein assembly · hollow capsules · noncovalent interactions · biofunctionalization · isobutyramide graft

The native properties of proteins, including biocompatibility, biodegradability, and biofunctionality, render them attractive for the fabrication of tailored architectures aimed at biomedical applications. The use of proteins in tissue engineering, biosensing, and drug delivery has led to significant interest in many areas aimed at studying and developing coatings,[1−6] capsules,[7−12] and self-assembled nanostructures.[13−17] Strategies for protein assembly can be classified into those that employ covalent and noncovalent interactions. Covalent cross-linking of protein assemblies can enhance their mechanical stability, as demonstrated by layer-by-layer (LbL)-assembled protein capsules cross-linked with glutaraldehyde.[18−20] However, the use of covalent cross-linkers leads to permanent bonds, preventing capsule disassembly, and, in some cases, has been shown to introduce cytotoxicity.[21−23] As an alternative, noncovalent interactions (*e.g.*, amphiphilic forces, electrostatic interactions, hydrogen bonding and/or hydrophobic interactions) have been extensively used for the preparation of various protein-based architectures, including self-assembled peptidic structures,[13−15,17,24] hydrogels,[25−28] films,[29,30] and particles.[31−33] Identifying novel combinations of noncovalent interactions between proteins and ligands, polymers or colloids will facilitate the development of next-generation protein-based architectures.

Human serum albumin (HSA, $M_w \approx 66$ kDa) is a globular protein composed of 585 amino acids and constitutes the most abundant protein in human blood plasma. The biofunctionality of HSA is related to its role in transporting nutrient molecules, which results from its various binding properties.[34,35] The biological nature and availability of HSA makes it a promising building block for the preparation of biocompatible, biodegradable, and nonimmunogenic carriers.[36,37] Several studies have investigated the formation of

* Address correspondence to fcaruso@unimelb.edu.au.

Received for review February 23, 2012 and accepted August 27, 2012.

Published online September 05, 2012
10.1021/nn302024t

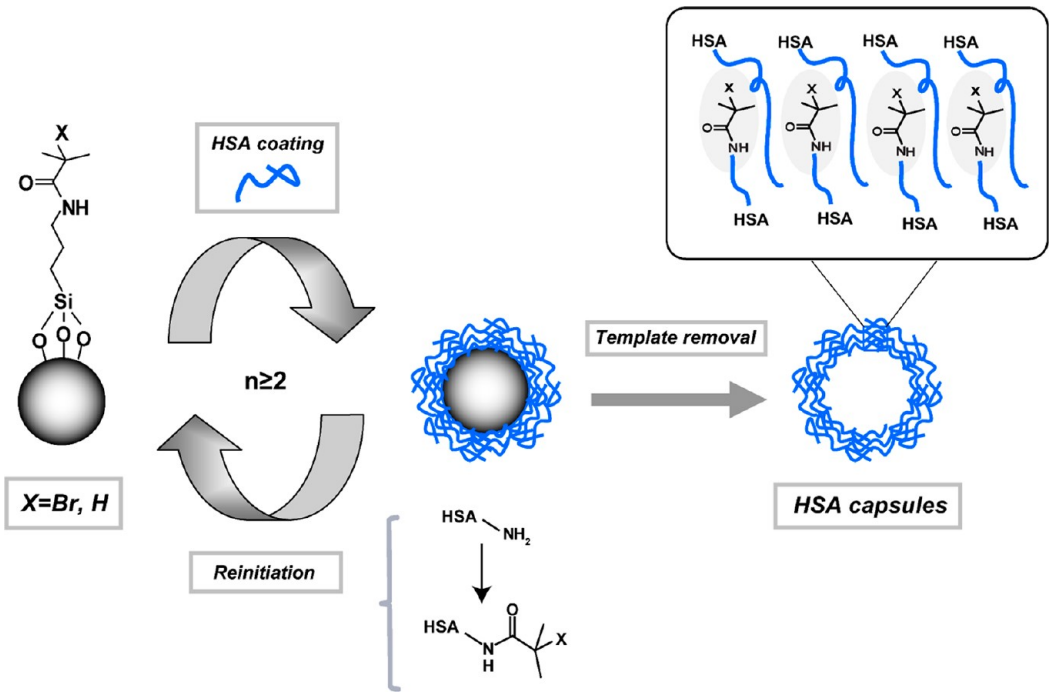

Scheme 1. Noncovalent protein assembly onto SiO_2 particles based upon the sequential adsorption of HSA and subsequent refunctionalization with BrIBAM or IBAM moieties to facilitate further protein adsorption. This process was repeated up to five times, leading to protein films with controlled growth profiles. Removal of the underlying template leads to stabilized protein capsules when two or more protein coating steps are performed. H-bonding (for IBAM and BrIBAM) and potentially halogen-bonding interactions with bromine (for BrIBAM) are proposed as the driving forces for the protein assemblies.

hollow capsules composed of HSA or bovine serum albumin (BSA) through noncovalent interactions. Lu *et al*. reported the one-step formation of *ca*. 100 μm diameter HSA microcapsules through the pendent drop technique.[38] The hollow HSA capsules were obtained by protein adsorption onto the surfaces of organic droplets produced at a chloroform/water interface at the tip of a capillary followed by evaporation of the organic phase. However, this process does not allow the size and thickness of such capsules to be tuned. An *et al*. reported the LbL electrostatic assembly of HSA and α-dimyristoyl-phosphatitic acid onto melamine formaldehyde resin or polystyrene colloidal particles to form lipid−protein microcapsules after core removal.[39,40] Detailed information was provided on the charge, thickness, and internal structure of the capsules, with further studies also demonstrating the pH-responsiveness of the protein−lipid capsules.[41] Recently, we reported a novel and versatile approach for the preparation of noncovalent protein and biopolymer free-standing architectures.[42] The process consists of the single-step adsorption of biopolymers onto silica particles chemically modified with bromoisobutyramide (BrIBAM: a brominated derivative of isobutyramide (IBAM)) followed by template removal. The driving force for assembly was demonstrated to be related to noncovalent interactions between the biopolymers and the BrIBAM moieties. Specifically, noncovalent interactions with the amide groups *via* H-bonding and with the bromine atoms *via* halogen bonding were suggested. While the formation of free-standing protein-based hollow capsules was achieved from a single protein coating step, the capsules displayed moderate mechanical stability. Furthermore, the film thickness was found to be related to the dimensions of the adsorbed biopolymer layer and as such could not be tuned.

Herein, we report the assembly of noncovalent protein films *via* the sequential adsorption of HSA intermittently refunctionalized with isobutyramide derivative grafts (BrIBAM or IBAM moieties) on silica (SiO_2) particles (Scheme 1). Moreover, after SiO_2 template removal, mechanically stable protein capsules with nanometer scale controlled thickness are obtained without the need for covalent cross-linking between the protein chains. Mechanically dispersible protein capsules in aqueous media are obtained from only two protein coating steps, which constitutes a significant gain in stability compared to polymer capsules formed by other methods. Protein capsules made *via* this process are shown to disassemble upon exposure to external stimuli, such as aqueous (urea) or organic (acetone) media. A network of H-bonds and possibly halogen-bonds may explain the formation of the thicker BrIBAM-HSA capsules compared to the IBAM-HSA capsules. Another advantage of the process is the versatile biofunctionalization, as is demonstrated by coating the protein capsules (IBAM-HSA and BrIBAM-HSA) with other biological macromolecules such as alkaline phosphatase (AP), dextran (DEX), and plasmid DNA (DNAp). The retention of biological functionality of such biopolymer hybrid capsules is shown

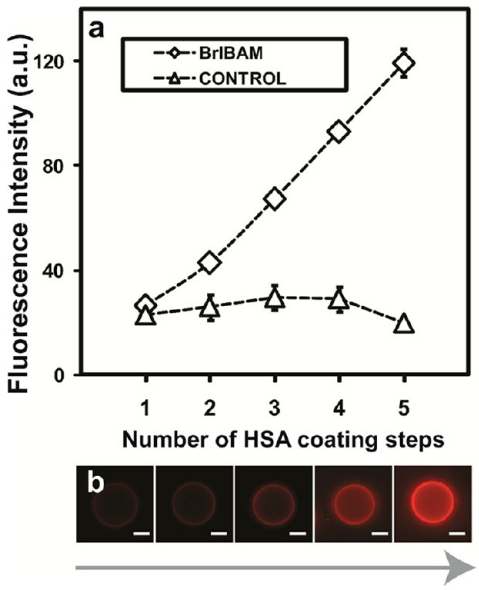

Figure 1. Growth of BrIBAM-HSA films on SiO_2 particles. (a) Evolution of the fluorescence intensity with increasing number of HSA-RITC coating steps, as followed by flow cytometry. (b) Fluorescence microscopy images of BrIBAM-HSA films deposited onto SiO_2 particles as a function of the number of HSA coating steps (from left to right, n = 1−5). Scale bars are 2 μm.

with AP-functionalized HSA capsules, which retain their enzymatic activity. Negligible cytotoxicity of the two types of protein capsules (*i.e.*, BrIBAM-HSA and IBAM-HSA) toward HeLa cells is demonstrated, and the influence of capsule wall thickness on capsule cellular association is reported.

RESULTS AND DISCUSSION

Formation of BrIBAM-HSA Capsules. Protein film growth through HSA adsorption and refunctionalization with BrIBAM moieties on nonporous silica (SiO_2) particles were followed by flow cytometry. Fluorescently labeled HSA-rhodamine isothiocyanate (RITC) was adsorbed for 30 min onto BrIBAM-modified SiO_2 particles (5 μm diameter) to generate the first protein coating. The protein surface was then functionalized with BrIBAM groups by the addition of an excess of 2-bromoisobutyryl bromide, which reacts with the pendent amine groups of the lysine or arginine residues of the protein, converting them into BrIBAM moieties. Subsequently, a second HSA coating was deposited over 30 min by adsorption onto the BrIBAM-functionalized HSA surface. This coating process was repeated up to five times to form a film denoted $(BrIBAM\text{-}HSA)_5$. Fluorescence intensity data obtained from flow cytometry (Figure 1a) illustrate the near-linear and continuous growth of the protein film on SiO_2 particles with increasing number of HSA coating steps. The initial fluorescence intensity of SiO_2 particles (26 ± 1 au) after the first HSA coating step (n = 1) increased by *ca.* 23 au increments per protein coating step until a final

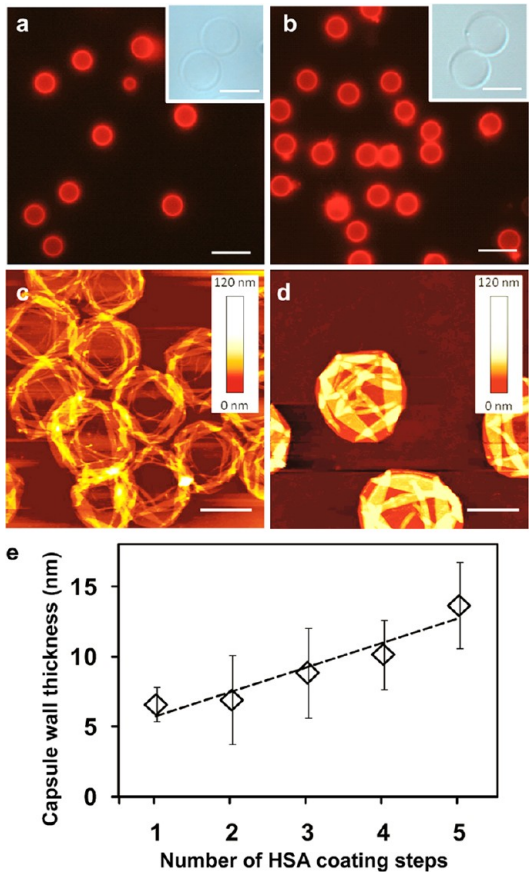

Figure 2. Fluorescence microscopy images of BrIBAM-HSA capsules initially templated onto 5 μm diameter SiO_2 particles after (a) n = 2 and (b) n = 5 HSA-RITC coating steps. Insets show bright field microscopy images of the capsules. AFM images of the BrIBAM-HSA capsules initially templated onto 3 μm diameter SiO_2 particles in the dried state after (c) n = 2 and (d) n = 5 HSA coating steps. (e) Evolution of the capsule wall thickness as a function of the number of HSA coating steps, as determined from AFM z-profile analysis. Scale bars are 10 μm for fluorescence microscopy images, 5 μm for bright field microscopy images, and 2 μm for AFM images.

fluorescence intensity of 119 ± 5 au was achieved after the fifth HSA coating step (n = 5). Flow cytometry experiments of control particles produced using the same conditions, but without intermittent functionalization of the surface with BrIBAM groups, revealed no significant increase in fluorescence intensity (Figure 1a), thus confirming the key role of the BrIBAM moieties in driving the assembly and growth of the protein film. Fluorescence microscopy images (Figure 1b) of the protein-coated particles after each HSA coating step reveal regular protein deposition onto the SiO_2 particles, as shown by the increase in the fluorescence of the particles with each coating step. Removal of the underlying SiO_2 template from the BrIBAM-HSA coated particles after each coating step (n = 2−5) yielded homogeneous and well-dispersed BrIBAM-protein hollow capsules with negligible shrinkage (see Figure 2a,b for fluorescence and bright field microscopy images of capsules after n = 2

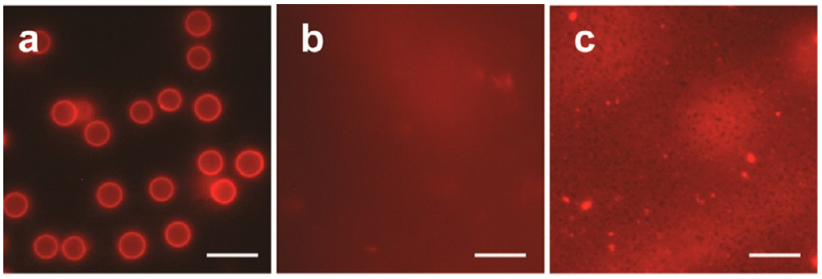

Figure 3. Disassembly of BrIBAM-HSA capsules imaged by fluorescence microscopy. $(BrIBAM\text{-}HSA)_3$ capsules (a) dispersed in water, (b) incubated with acetone (*ca.* 1 min), and (c) incubated with urea (3 M aqueous solution) (*ca.* 4 h). Scale bars are 10 μm.

and 5 coating steps). Atomic force microscopy (AFM) images (Figure 2c,d) of the protein capsules in the dried state for $n = 2$ and 5 HSA coating steps show homogeneous structures with significantly higher densities compared with our previously reported capsules prepared by a single HSA adsorption step onto BrIBAM modified surfaces.[42] The capsule wall thickness with HSA coating step (Figure 2e), as determined by AFM *z*-profile analysis (Supporting Information, Figure S1), linearly increases, which is consistent with the flow cytometry data and fluorescence microscopy images (Figure 1). The wall thickness of the protein capsules ranged from *ca.* 6 $\pm$ 2 nm for the first HSA coating to *ca.* 14 $\pm$ 3 nm after five HSA coatings, with an average thickness increment of *ca.* 2 nm per HSA coating (for $n = 1-5$). Uniform film growth is attributed to a regular and consistent functionalization of the protein lysine or arginine groups with BrIBAM moieties after each HSA coating step.

Previously, we demonstrated that BrIBAM interactions with proteins and other biopolymers occur through noncovalent interactions and that both the isobutyramide and bromine substituted BrIBAM moieties play a role in the cohesive process.[42] Therefore, the noncovalent nature of the sequential BrIBAM-HSA capsules was investigated by assessing their intermolecular disassembly. $(BrIBAM\text{-}HSA)_3$ capsules were incubated with solutions of either acetone or urea (3 M aqueous solutions). In both cases, complete disassembly was observed with protein release into solution occurring rapidly with acetone (<1 min) and more slowly with urea (*ca.* 4 h) (Figure 3). These results are similar to those we previously reported for BrIBAM-HSA capsules obtained with one HSA coating step, confirming that the interactions between HSA and BrIBAM-functionalized HSA are noncovalent in nature and are readily disrupted by acetone or urea.

BrIBAM *versus* IBAM. The role of the bromine atoms attached to the isobutyramide groups in the assembly of the protein films was experimentally assessed by using the bromine-free IBAM groups. Thus, the same procedure as that described for the BrIBAM studies was employed, with the exception that isobutyryl chloride was used in place of 2-bromoisobutyryl bromide. Initially, HSA was adsorbed onto IBAM-functionalized SiO_2 particles and then the lysine and arginine groups of the surface-coated protein were refunctionalized with IBAM groups *via* reaction with isobutyryl chloride followed by further protein adsorption. The protein film growth *via* HSA adsorption and IBAM refunctionalization was followed by flow cytometry (Figure 4a). Similar to the BrIBAM system, a near-linear increase in fluorescence intensity with increasing number of HSA coating steps was monitored. However, comparison of the fluorescence intensity increments obtained per coating step from flow cytometry for the BrIBAM and IBAM systems (performed with the same acquisition parameters) indicates a significantly lower slope for the IBAM system (*ca.* 13 au) compared to the BrIBAM system (*ca.* 23 au). Over five coating steps, the fluorescence intensity of the $(IBAM\text{-}HSA)_5$ films (78 $\pm$ 4 au) was *ca.* 30% less than that for the $(BrIBAM\text{-}HSA)_5$ films. These results suggest that the IBAM approach is suitable for the assembly and growth of protein films, although significantly less protein is adsorbed (30% less after five coating steps) compared with the BrIBAM approach. Removal of the SiO_2 templates from the IBAM-HSA coated particles for $n = 2$ and 5 yielded homogeneous and well-dispersed HSA hollow capsules with negligible shrinkage (Figure 4b,c and Supporting Information, Figure S2). AFM images recorded in the dried state (Figure 4e,f) show homogeneous capsules (for $n = 2$ and 5 HSA coating steps). AFM *z*-profile analysis (Supporting Information, Figure S3) revealed thinner capsule walls (see thickness graph in Figure 4d) for the IBAM-HSA capsules (5.5 $\pm$ 2 nm for $n = 2$, 10 $\pm$ 2 nm for $n = 5$) compared to their BrIBAM-HSA analogues (7 $\pm$ 3 nm for $n = 2$, 14 $\pm$ 3 nm for $n = 5$) (Figure 2c,d). Interestingly, when only one HSA coating is assembled on IBAM-modified SiO_2 particles, capsules are not observed (Figure S4). In contrast, two HSA coatings yield $(IBAM\text{-}HSA)_2$ capsules and may constitute a suitable alternative to BrIBAM-HSA capsules when the presence of bromine atoms is not desired. IBAM-mediated binding most likely results from a dense network of hydrogen bonds between the IBAM moieties and the peptide backbone of the proteins. The flow cytometry results and AFM analysis clearly emphasize the simultaneous roles of the amide and bromide functionalities to form noncovalent

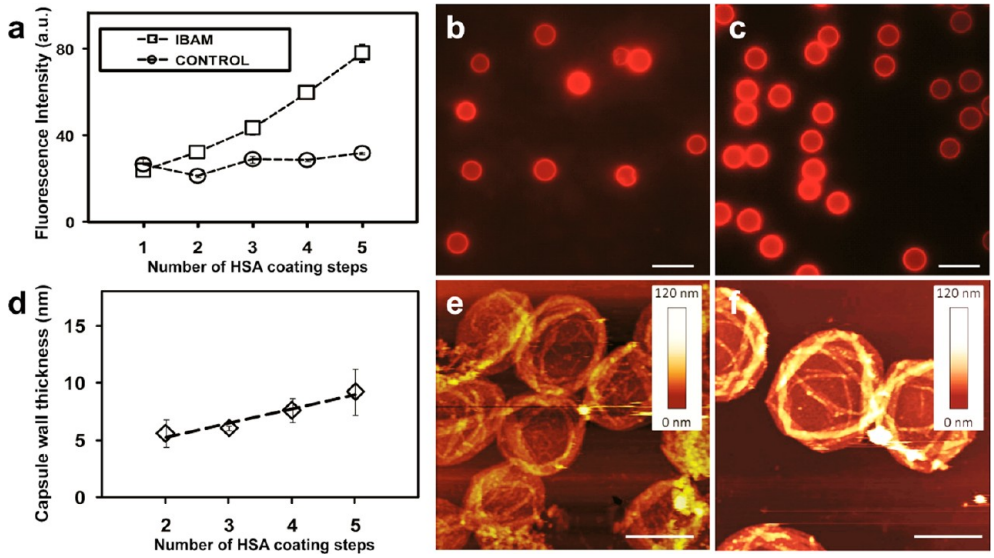

Figure 4. Growth of IBAM-HSA films and capsules. (a) Evolution of the fluorescence intensity with increasing number of HSA-RITC coating steps on SiO_2 particles, as followed by flow cytometry. Fluorescence microscopy images of IBAM-HSA capsules initially templated onto 5 μm diameter SiO_2 particles after (b) $n = 2$ and (c) $n = 5$ HSA-RITC coating steps. (d) Evolution of the capsule wall thickness as a function of the number of HSA coating steps, as determined from AFM z-profile analysis. AFM images of IBAM-HSA capsules initially templated onto 3 μm diameter SiO_2 particles in the dried state after (e) $n = 2$ and (f) $n = 5$ HSA coating steps. Scale bars are 10 μm for fluorescence microscopy images and 2 μm for AFM images.

interactions generated within the BrIBAM-HSA and IBAM-HSA assemblies.

To assess the wettability of the BrIBAM and IBAM grafts, water contact angle measurements of silicon slides grafted with BrIBAM and IBAM moieties were performed. Similar values of $52 \pm 3°$ and $56 \pm 1°$ were measured for the BrIBAM and IBAM films, respectively, whereas blank silicon slides (control experiments) possessed a lower contact angle value of $22 \pm 2°$ (Supporting Information, Figure S5). These results demonstrate that BrIBAM and IBAM grafts have a similar and quite significant hydrophobicity, and that the Br atom from the BrIBAM moiety does not increase the hydrophobicity of the films.

Noncovalent Interactions. Recently, the implication of the larger halogen atoms (Cl, Br, and I) in the formation of halogen bonds that are able to compete with hydrogen bonds in biological systems has been assessed.[43−50] Here, we calculated the electrostatic potential surfaces of bromine and hydrogen atoms by using the Hartree−Fock quantum model (Figure 5a,b) for the BrIBAM and IBAM compounds. A positive value of the electrostatic potential (50 kJ mol^{-1}) calculated at the top of the bromine atom reveals an electron-deficient region (referred to as a "sigma-hole") that is able to interact favorably with electron donating groups such as oxygen atom lone pairs characteristic of carbonyl groups.[43] In comparison, alkyl hydrogen atoms, such as the methine proton from IBAM, are not able to establish strong bonding interactions with electron donors. This suggests that the bromine extremity of BrIBAM behaves as a Lewis acid that may interact with electron donors present in the HSA proteins. Moreover, such atomic charge distribution is very similar to that obtained with models of halogenated compounds forming halogen bonds with proteins. Numerous electron donor atoms are present in the polypeptide chains of proteins (N, O, and S) and the most common halogen-bonds encountered between proteins complexed with halogenated compounds involve the oxygen atoms on the protein carbonyl groups.[43,47−49] A recent X-ray crystallography study on dibromo-amide modified taxane bound to tubulin revealed a short and highly directed Br−O contact (3.17 Å, angle C−Br···O of 173°) that was identified as a halogen-bond.[50] Figure 5c shows the electrostatic potential surfaces of the dibromo-amide modified taxane that were mapped *via* the same Hartree−Fock model used above. Comparison of the electrostatic potential surfaces for the bromine atom of the dibromo-amide modified taxane forming a halogen-bond with BrIBAM indicates very similar atomic charge distributions and values of electrostatic potential (*ca.* 51 kJ mol^{-1} calculated at the top of the bromine). As a result of the theoretical insights obtained through these calculations and data gathered from the literature, we postulate that bromine atoms play a role, through halogen-bonding, in the formation of the thicker BrIBAM-HSA films (~30%) when compared with IBAM-HSA films.

Biofunctionalization. Biofunctionalization of the BrIBAM-HSA and IBAM-HSA protein films with other biological macromolecules after subsequent reinitiation with BrIBAM or IBAM grafts was investigated with fluorescently labeled alkaline phosphatase (RITC-labeled, AP-RITC), dextran (fluorescein isothiocyanate-labeled, DEX-FITC) and DNA plasmid (stained with

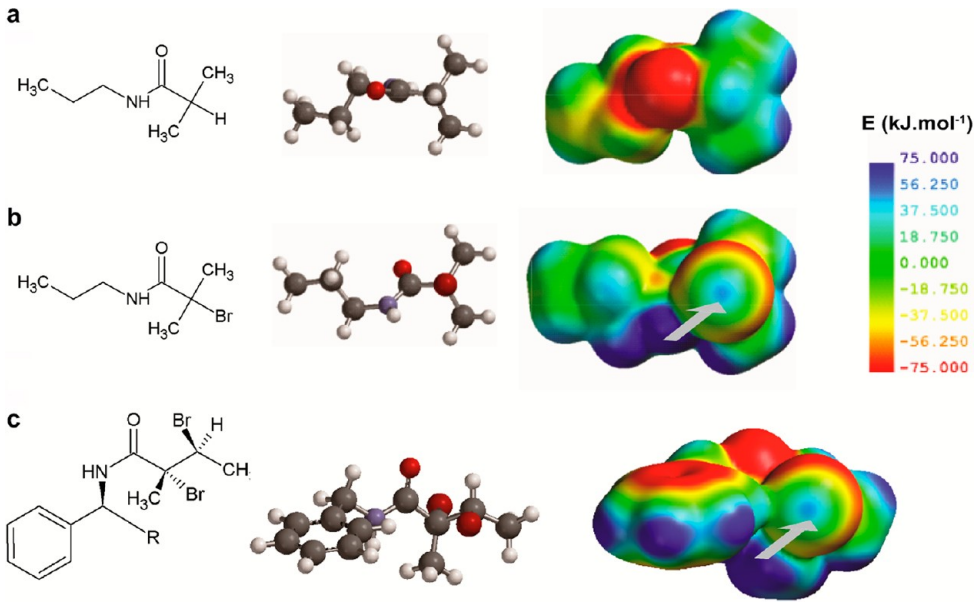

Figure 5. Chemical structures (Lewis and 3D) and *ab initio* electrostatic potential surfaces of (a) an IBAM moiety, (b) a BrIBAM moiety, and (c) a dibromo-amide modified taxane establishing an halogen-bond within tubulin (3.17 Å, angle C−Br···O of 173°).[45] The C−H (IBAM) and equivalent C−Br (BrIBAM) bonds are shown perpendicular to the page. The C−Br bonds of the dibromo-amide modified taxane are also shown perpendicular to the page and the Br establishing a halogen-bond is represented in the front. R represents a part of the brominated taxane molecule distant from the halogen bond. The potential energies are presented in the −75 to +75 kJ mol^{-1} range to emphasize the variation in electrostatic potential associated with the halogen atom. The gray arrows point to positive electrostatic potentials at the apex of the bromine atoms and are indicative of the presence of an electron-deficient region (also referred to as a sigma-hole) that are able to establish favorable interactions with electron donating groups such as the lone pairs of carbonyl groups.

green fluorescent YOYO-1, a high affinity nucleic acid stain, DNAp-YOYO). Flow cytometry experiments performed on SiO_2 templates (Figure 6a) coated with $(BrIBAM\text{-}HSA)_4$ or $(IBAM\text{-}HSA)_4$ protein films indicate that the three biopolymers AP, DEX, and DNAp adsorbed onto the reinitiated protein surface. Moreover, significantly less biopolymer was adsorbed when coated onto IBAM surfaces compared to BrIBAM surfaces (*ca.* 30, 50, and 35% less for AP, DEX, and DNAp, respectively). These results are consistent with the presence of a higher amount of the BrIBAM grafts (compared to IBAM) resulting from a higher protein quantity and thickness, as observed above. Better retention of the biopolymers due to possible interactions with the bromine atoms may also explain this effect. Figure 6b,d show the resulting $(BrIBAM\text{-}HSA)_4$ capsules functionalized with AP, DEX, and DNAp, respectively. Similar biofunctionalized IBAM-HSA capsules were also obtained (Supporting Information, Figure S6). Retention of the biological functionality of the adsorbed outer layer was assessed using AP-functionalized BrIBAM-HSA capsules. The continuous and linear conversion of *p*-nitrophenylphosphate (PNP) into *p*-nitrophenol (PN) catalyzed by the AP-functionalized BrIBAM-HSA capsules and followed in solution by UV/Vis spectrophotometry (at $\lambda = 410$ nm, maximum absorption of PN) demonstrates that the absorbed AP enzymes retain their activity (Figure 6e). Control experiments without any AP coating indicated that neither BrIBAM grafts nor HSA protein promoted the conversion of PNP into PN. The enzymatic activity of the equivalent amount of alkaline phosphatase with that contained in the AP-functionalized BrIBAM-HSA capsules was also investigated in bulk solution (see details in Supporting Information, Figure S7). The reaction kinetics were found to be considerably faster (*ca.* 150 times) compared with the AP-functionalized BrIBAM-HSA capsules. This effect may be explained by the fact that for the free enzyme in bulk solution, the enzymatic sites are more accessible compared to enzymes and HSA associated within the protein capsule wall.

Cytotoxicity Studies. Smaller SiO_2 particle templates (1.11 and 0.585 μm diameter) were employed for the formation of HSA capsules with more suitable sizes for biomedical applications and cellular interactions[36,51,52] (*i.e.*, ≤ 1 μm). The same process as described previously was employed to prepare $(BrIBAM\text{-}HSA)_4$ and $(IBAM\text{-}HSA)_4$ capsules. After template removal, the capsules were well-defined and readily dispersed in aqueous buffer, thus demonstrating the versatility of the process to tune the size of the capsules. Transmission electronic microscopy (TEM) images of these capsules in the dried state confirmed homogeneous structures with diameters of *ca.* 1 and 0.5 μm for both BrIBAM-HSA (Figure 7a,b) and IBAM-HSA (Figure 7c,d) capsules. To assess the effect of these BrIBAM-HSA and IBAM-HSA capsules on cell viability, an MTT assay was conducted by incubating various doses of the two types of HSA capsules (with sizes of 1 and 0.5 μm) with HeLa cells (Figure 7e). The results demonstrate that even at a

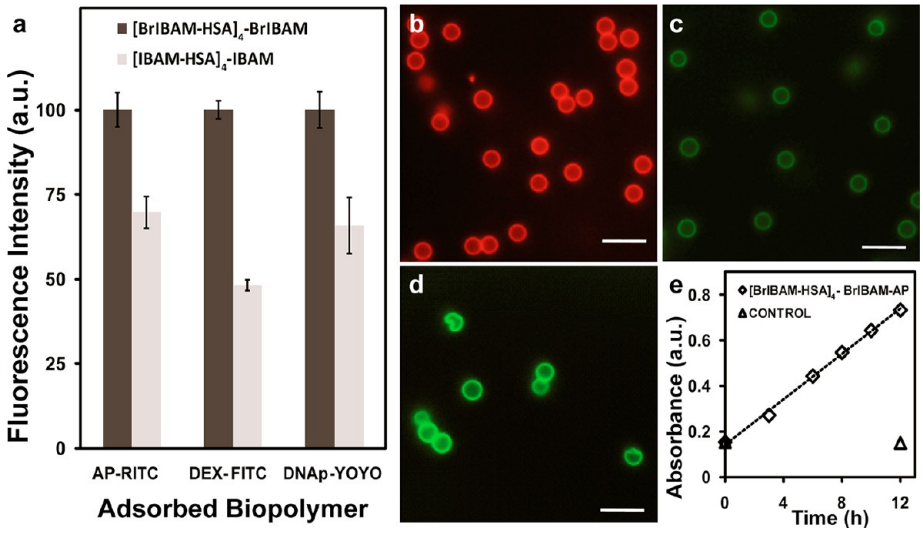

Figure 6. Biofunctionalization of BrIBAM-HSA and IBAM-HSA protein films with biological macromolecules. (a) Comparison followed by flow cytometry of the relative adsorption content of AP, DEX, and DNAp adsorbed onto $(BrIBAM\text{-}HSA)_4$-BrIBAM and $(IBAM\text{-}HSA)_4$-IBAM protein films coated onto silica templates. Fluorescence intensities are normalized for clarity. Fluorescence microscopy images of $(BrIBAM\text{-}HSA)_4$-BrIBAM capsules functionalized with (b) AP-RITC, (c) DEX-FITC, and (d) DNAp-YOYO. Scale bars are 8 μm. (e) Kinetic plot of the conversion of PNP into PN and a phosphate ion catalyzed by the $(BrIBAM\text{-}HSA)_4$-(BrIBAM-AP) capsules and followed by UV/Vis spectrophotometry at 410 nm.

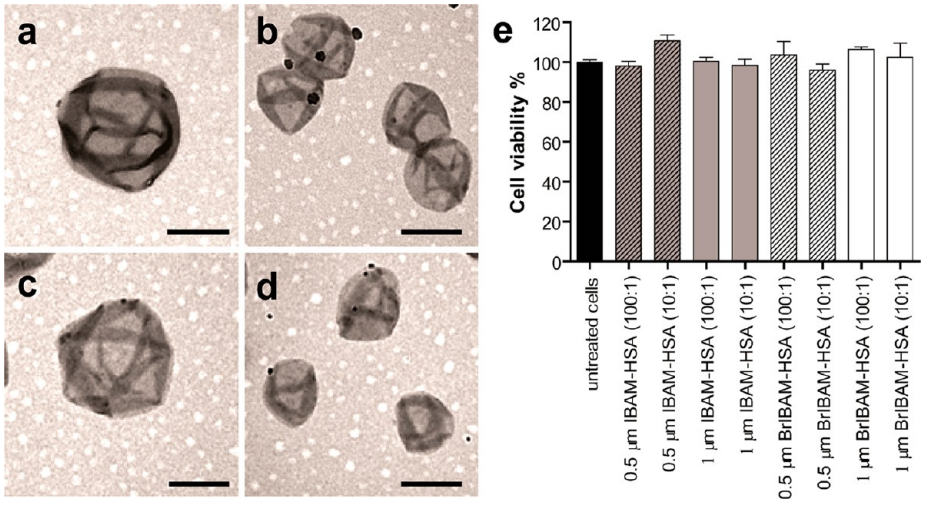

Figure 7. TEM images of $(BrIBAM\text{-}HSA)_4$ capsules with diameters of (a) 1 and (b) 0.5 μm. TEM images of $(IBAM\text{-}HSA)_4$ capsules with diameters of (c) 1 and (d) 0.5 μm. Scale bars are 0.5 μm. (e) Cell viability of HeLa cells incubated with $(IBAM\text{-}HSA)_4$ (0.5 and 1 μm diameter) and $(BrIBAM\text{-}HSA)_4$ (0.5 and 1 μm diameter) capsules at different capsule/cell ratios (100:1 and 10:1) for 24 h, as measured by an MTT assay. Cell viability is normalized as a percentage of untreated cells. The data are presented with the mean and standard error of two independent experiments, each performed in triplicate.

high dose (*ca.* 100 capsules per cell), the cell viability and metabolic activity after an incubation period of 24 h are not significantly affected by the capsules (compared with untreated cells), suggesting no significant cytotoxicity. Following this initial study on cell viability in the presence of the capsules, further investigations *in vitro* and *in vivo* will be required to fully assess the biocompatibility of these capsules.

Cellular Association with BrIBAM-HSA Capsules. We next investigated the effect of capsule wall thickness on cellular association. AlexaFluor (AF) 488-labeled BrIBAM-HSA capsules (1 μm in diameter) with different HSA layer numbers (from 2 to 5) were incubated with HeLa cells at a capsule-to-cell ratio of 100:1. The extent of cellular association at 6 and 24 h was evaluated using flow cytometry. It was shown that approximately 32% and 63% of the cells were associated with $(BrIBAM\text{-}HSA)_2$ capsules after incubation for 6 and 24 h, respectively, which is significantly higher than the other multilayered $(BrIBAM\text{-}HSA)_n$ capsules with $n = 3-5$ for the same time periods (Figure 8a). The higher extent of $(BrIBAM\text{-}HSA)_2$ capsule internalization was confirmed by deconvolution fluorescence microscopy imaging. Microscopy images show that significantly

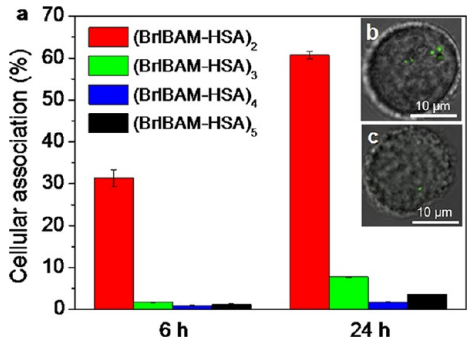

Figure 8. Interaction of AF488-labeled BrIBAM-HSA capsules composed of different layer numbers with HeLa cells for 6 and 24 h incubation at 37 °C. (a) Percentage of cells associated with capsules was quantified by flow cytometry. Data are the mean ± standard deviation. At least 5000 cells were analyzed in each experiment. Representative images of cells internalized with (b) $(BrIBAM-HSA)_2$ or (c) $(BrIBAM-HSA)_5$ capsules are shown.

more $(BrIBAM-HSA)_2$ capsules (Figure 8b) were internalized in HeLa cells compared with $(BrIBAM-HSA)_5$ capsules (Figure 8c). Previous studies have demonstrated that the internalization of hollow capsules involves capsule deformation.[53,54] Furthermore, Fery *et al.* reported that the stiffness of polyelectrolyte capsule shells is proportional to the square of the shell thickness.[55,56] We postulate that the $(BrIBAM-HSA)_2$ capsules are the most flexible among the series of HSA capsules studied, favoring deformation and resulting in enhanced cellular uptake. Taken together, these results show that the sequential assembly of HSA capsules *via* BrIBAM grafts affords control over cellular uptake of the capsules. This opens the way for possibilities in biomedical applications, such as targeted drug delivery, where the balance between improved biodistribution and high rate of drug administration are closely linked with cellular uptake.

CONCLUSION

The preparation of sequentially assembled noncovalent protein films based on the physical adsorption of HSA and chemical refunctionalization with isobutyramide grafts (*i.e.*, isobutyramide or bromoisobutyramide) was reported. This approach allows for the formation of protein films with controlled growth profiles onto silica particles that, after template removal, yield hollow protein capsules with controllable wall thicknesses. These protein capsules displayed no significant cytotoxicity toward HeLa cells and their capsule wall thickness was found to influence their cellular uptake of HSA capsules, suggesting that the sequential assembly approach has significant potential for tailored cell studies. Versatile biofunctionalization of such protein capsules was demonstrated with the efficient formation of AP-, DEX-, and DNA plasmid-coated protein capsules that maintain biofunctionality, as demonstrated with AP-functionalized BrIBAM-HSA capsules. On the basis of the differences observed for the BrIBAM-HSA and IBAM-HSA systems, the driving force for protein assembly was hypothesized to result from a network of hydrogen- and halogen-bonding interactions arising from the amide groups and bromine atoms, respectively. Understanding the processes associated with the cohesion of such protein assemblies is of primary importance to develop smart bioresponsive materials. Current investigations are focused on elucidating the local structure of the protein films, including the degree of organization and electronic environment at the molecular/atomic level around the BrIBAM and IBAM moieties. In addition, functionalization of the capsules with cell-targeting biomolecules (*e.g.*, sugars or aptamers) and therapeutic drugs is under investigation.

METHODS

Materials. 3-Aminopropyltriethoxysilane (APTS), ethanol (EtOH), ammonium hydroxide solution (28 wt % in water), isobutyryl chloride (IBC), 2-bromoisobutyryl bromide (BrIB), triethylamine (Et_3N), *N*,*N*-dimethylformamide (DMF), rhodamine B isothiocyanate (RITC), sodium bicarbonate ($NaHCO_3$), dimethylsulfoxide (DMSO), acetone, urea, hydrofluoric acid (HF, 48 wt % in H_2O), ammonium fluoride, poly(ethylene imine) (PEI), human serum albumin (HSA), alkaline phosphatase (AP) from bovine intestinal mucosa, *p*-nitrophenylphosphate (PNP), and FITC labeled dextran (FITC-DEX) (M_w = 70 kDa) were obtained from Sigma-Aldrich and used as received. DNA plasmid (DNAp) was provided by A.W. Püschel (Münster Universität, Germany) (pBK-ha-NRP1). Nonporous silica particles of various sizes (5 wt % suspensions, average diameters of 5.35, 3.25, 1.11, and 0.585 μm) were obtained from Microparticles GmbH (Berlin, Germany). YOYO-1 iodide DNA-stain, Dulbecco's modified eagle medium (DMEM), fetal bovine serum (FBS), Alexa Fluor 488 carboxylic acid, succinimidyl ester (AF488), Dulbecco's phosphate-buffered saline (DPBS), and (3-(4,5-dimethylthiazol-2-yl)-2,5-diphenyltetrazolium bromide) (MTT) were purchased from Invitrogen and used as received.

Fluorescent Labeling of HSA and AP. HSA was fluorescently labeled with RITC using a HSA:RITC mole ratio of 1:2. RITC was dissolved in DMSO (10 mg mL^{-1}) and gently mixed with a solution of HSA (10 mg mL^{-1}) dissolved in 0.1 M $NaHCO_3$ buffer (pH 8.5) for 1 h. An identical procedure was employed for AP-RITC. HSA-RITC and AP-RITC were purified by size exclusion chromatography (SEC). The SEC column was equilibrated with Milli-Q water (20 mL) and then loaded with the concentrated protein solutions. The purified HSA-RITC and AP-RITC were then collected by eluting with Milli-Q water. For cell association experiments, HSA was labeled with AF488. Briefly, 30 mg of HSA was dissolved in 50 mM PBS buffer (pH 7.4). The mixture was stirred for 3 h and dialyzed against Milli-Q water to purify the AF488-labeled HSA. The labeled HSA was freeze-dried and stored at 4 °C before use.

Bromoisobutyramide (BrIBAM)- and Isobutyramide (IBAM)-Modified Silica Particles. Nonporous silica particles (200 μL, 5 wt % in EtOH) were dispersed in a solution of EtOH (500 μL) containing ammonium hydroxide solution (30 μL, 30 wt % in water) and APTS (125 μL). After 2 h, the amino-modified particles were isolated *via* centrifugation and washed with EtOH (1 × 200 μL) and DMF (3 × 200 μL). A solution containing BrIB (65 μL) in anhydrous DMF(400 μL) was added dropwise to the amino-modified silica

particles previously dispersed in a solution of DMF (400 μL) and Et_3N (40 μL). After 2 h, Milli-Q water (200 μL) was added to dissolve the formed precipitates, and the resulting particles were isolated *via* centrifugation and washed with DMF (3 × 200 μL). The same procedure was used to prepare IBAM-modified silica particles with the exception that IBC (55 μL) was used in place of BrIB.

Protein Coating and Refunctionalization Processes. BrIBAM- and IBAM-modified silica particles dispersed in DMF (100 μL, 5 wt %) were added to aqueous solutions of HSA-RITC (1.0 mL, 0.25 mg mL^{-1}) and allowed to stand for 30 min, followed by centrifugation and washing with Milli-Q water (1 mL). The resulting BrIBAM-HSA and IBAM-HSA coated particles (n = 1 coating step) were washed with anhydrous DMF (3 × 100 μL) and redispersed in a solution of DMF (200 μL) and Et_3N (20 μL). Separately, BrIB (32 μL) and IBC (27 μL) were dissolved in DMF (200 μL) and slowly added to the previously dispersed BrIBAM-HSA and IBAM-HSA coated particles, respectively. After 2 h, Milli-Q water (100 μL) was added to dissolve the formed precipitates and the resulting particles were isolated *via* centrifugation and washed with DMF (3 × 100 μL). A second HSA coating step was performed by addition of the particles to a fresh solution of HSA-RITC (1.0 mL, 0.25 mg mL^{-1}) in Milli-Q water for 30 min followed by centrifugation and washing with Milli-Q water (1 mL). After analysis, these HSA-coated particles (n = 2 coating steps) were refunctionalized with BrIBAM and IBAM moieties and HSA coating was repeated according to the above procedure to afford particles with up to five HSA coatings (n = 5).

Biofunctionalization. $(BrIBAM\text{-}HSA)_4$ coated particles were first refunctionalized with BrIBAM moieties *via* the protocol described above and subsequently biofunctionalized by the adsorption (1 h) of AP-RITC (0.5 mg mL^{-1}), DEX-FITC (0.5 mg mL^{-1}), or DNAp (0.1 mg mL^{-1}) in Milli-Q water (1 mL) followed by centrifugation and washing with Milli-Q water (1 mL). YOYO-1 aqueous solution (10000 fold dilution) as a green fluorescent DNA stain was added for 20 min to the $(BrIBAM\text{-}HSA)_4$-BrIBAM-DNAp coated particles (0.1 wt %) followed by particle washing with Milli-Q water. $(IBAM\text{-}HSA)_4$ coated particles were refunctionalized with IBAM moieties and biofunctionalized *via* the same procedure.

Preparation of HSA and HSA-biopolymer (AP, DEX, or DNA) Capsules. *Caution! This method utilized HF which is highly toxic and great care must be taken when handling.*

For one HSA coating (n = 1), the BrIBAM-HSA coated particles (1 μL, 0.5 wt %) were deposited onto a PEI-coated slide (glass, silicon, or gold wafer) and brought into contact with ammonium fluoride (8 M) buffered HF (2 M) (NH_4F/HF, 1 μL, pH 5) for 1 min, followed by extensive rinsing of the slide with Milli-Q water. For $n \geq 2$ HSA coating steps (n = 2–5), BrIBAM-HSA coated particles (100 μL, 1 wt %) and IBAM-HSA coated particles (100 μL, 1 wt %) were added to ammonium fluoride (250 μL, 8 M) buffered HF (2 M, pH 4) and mixed very gently for 2 min. The resulting capsules were then centrifuged at low speed (1800–2000 *g*) for 15 min and washed with Milli-Q water (3 × 50 μL). The process is identical to that used for the HSA-biopolymer capsules.

Measurement of Enzymatic Activity of HSA-AP Capsules. Enzymatic activity of $(BrIBAM\text{-}HSA)_4$-BrIBAM-AP capsules was detected by using *p*-nitrophenylphosphate (PNP). The PNP solution (1 mL) at a concentration of 1.7 mg mL^{-1} in 0.05 M $NaHCO_3$ buffer (pH = 8.5) was brought in contact with the $(BrIBAM\text{-}HSA)_4$-BrIBAM-AP capsules and the subsequent formation of *p*-nitrophenol (PN) and a phosphate ion by enzymatic conversion of PNP was followed by UV/Vis spectrophotometry at λ = 410 nm (maximum absorption).

Cell Viability Experiments. HeLa cells were cultured in DMEM media containing 10% FBS at 37 °C in a humidified atmosphere containing 5% CO_2. Cell viability was measured by reduction of MTT, as described previously.[57] Briefly, HeLa cells were seeded at 5 × 10^3 cells/well in 96-well plates and incubated with capsules at various ratios in 200 μL of growth media for 24 h. After treatment, cells were further incubated with fresh medium containing MTT (0.5 mg mL^{-1}) for 4 h. The resulting blue formazan was solubilized using 150 μL of acidified isopropyl alcohol (0.04 N HCl), and the absorbance at 570 nm was measured with a plate reader (Multiskan Ascent, Thermo Scientific). The cell viability of treated cells was normalized as a percentage of untreated cells. The mean ± the standard errors were calculated from two independent experiments performed in triplicate.

Cellular Association Experiments. HeLa cells were plated at 7.5 × 10^4 cells/well in 24-well plates. AF488-labeled HSA capsules with various layers of HSA (from 2 to 5 layers) were added to the cells at a capsule-to-cell ratio of 100:1. The cells were incubated with the capsules at 37 °C for 6 and 24 h. After the treatment, the cells were washed with DPBS three times, trypsinized, and resuspended in DPBS. The cellular association was analyzed by flow cytometry. Experiments were performed in duplicate, and at least 5000 cells were analyzed in each experiment.

Characterization Methods. *Flow Cytometry.* A Cyflow Space (Partec GmbH) flow cytometer using an excitation wavelength of 488 nm (emission filter of 560–590 nm) was used to follow the growth of the BrIBAM-HSA-RITC and IBAM-HSA-RITC films on silica particles in Milli-Q water (pH 5.8). Flow cytometry graphs show evolution of fluorescence intensity (au) with the number of HSA coating steps. At least 20000 particles were analyzed in each experiment. A Miltenyi flow cytometer using an excitation wavelength of 488 nm (emission filters of 490–520 nm and 560–590 nm) was used to compare the relative amount of fluorescently labeled AP-RITC, DEX-FITC, and YOYO-1 stained DNAp onto $(BrIBAM\text{-}HSA)_4$ and $(IBAM\text{-}HSA)_4$ coated silica particles. At least 20000 particles were analyzed in each experiment.

Bright Field and Fluorescence Microscopy. Images of the protein-coated silica particles and protein capsules were taken using an Olympus IX71 inverted fluorescence microscope equipped with a DIC slider (U-DICT, Olympus), the corresponding filter sets, and a 60× oil immersion objective (Olympus UPFL20/0.5NA, W.D. 1.6).

Atomic Force Microscopy (AFM). The imaged protein capsules were deposited onto PEI-coated silicon wafers, rinsed extensively with Milli-Q water, and allowed to air-dry. AFM scans of the capsules were carried out with a JPK NanoWizard2 BioAFM and with a D3000 Nanoscope IIIa (Veeco, Santa Barbara, CA). Typical scans were conducted in intermittent contact mode (AC mode) with silicon cantilevers (NSC/CSC) (MikroMasch, Bulgaria) using the accompanying JPK image processing software and in contact mode with a silicon nitride tip (model MSCT-AUHW, Veeco, Santa Barbara, CA) using the accompanying Veeco processing software.

Contact Angle Measurements. Contact angle was measured on a Digidrop (Romans, France) apparatus. Three droplets of pure water (2 μL) were deposited and analyzed for each sample.

UV/Vis Spectrophotometry. A SAFAS (Monaco) spectrophotometer was used to measure evolution of the absorbance as a function of the time of *p*-nitrophenol (PN) formation catalyzed by the $(BrIBAM\text{-}HSA)_4$-BrIBAM-AP capsules in $NaHCO_3$ buffer solution (pH 8.5, 0.05 M).

Transmission Electron Microcopy (TEM). HSA capsules were deposited onto Formvar-coated copper grids, rinsed extensively with Milli-Q water, and allowed to dry in air. TEM analysis was carried out with a Philips CM120 BioTWIN instrument operated at 120 kV.

Theoretical Study: Mapping of Electrostatic Potential Surface (Hartree–Fock Model). The methodology used here is similar to that used in a study describing the importance of halogen bonds in biological systems.[48] Molecular models of the BrIBAM and IBAM moieties were constructed and their geometries optimized at the 3-21G$^{(*)}$ Hartree–Fock level (Figure 5). Electrostatic potential surfaces were generated by mapping the 3-21G$^{(*)}$ electrostatic potentials onto surfaces of molecular electron density (0.002 electron per Å^3) by using the SPARTAN program (Wave function, Irvine, CA). Note that the 3-21G$^{(*)}$ basis set was used because the 6-31G$^{(*)}$ basis set and above are incomplete for bromine atoms. The limitations related to the use of electrostatic potential surfaces are discussed at length by Mecozzi *et al.* who demonstrated their usefulness in providing quantitative guidelines for evaluating the ability of aromatic compounds to form cation–π interactions.[58]

Conflict of Interest: The authors declare no competing financial interest.

Acknowledgment. This work was supported by the Australian Research Council under the Discovery (F.C.) and Federation

Fellowship (F.C.) schemes. We thank R. Curtain, A. Grant, and T. Gengenbach for helpful discussions regarding analysis techniques. F. Boulmedais, P. Schaaf and J. Best are thanked for helpful discussion. J. Aitken is acknowledged for preliminary analysis of EXAFS spectra performed at the Australian Synchrotron, Melbourne.

Supporting Information Available: AFM images and *z*-profile analysis of BrIBAM-HSA and IBAM-HSA capsules, bright field images of IBAM-HSA capsules, contact angle measurements, fluorescence microscopy images of IBAM-HSA biofunctionalized capsules with AP, DEX, and DNAp and enzymatic activity of alkaline phosphatase in solution. This material is available free of charge *via* the Internet at http://pubs.acs.org.

REFERENCES AND NOTES

1. Vörös, J. The Density and Refractive Index of Adsorbing Protein Layers. *Biophys. J.* **2004**, *87*, 553–561.
2. Hook, F.; Vörös, J.; Rodahl, M.; Kurrat, R.; Boni, P.; Ramsden, J. J.; Textor, M.; Spencer, N. D.; Tengvall, P.; Gold, J.; *et al.* A Comparative Study of Protein Adsorption on Titanium Oxide Surfaces Using *in Situ* Ellipsometry, Optical Waveguide Lightmode Spectroscopy, and Quartz Crystal Microbalance/Dissipation. *Colloids Surf., B-Biointerfaces* **2002**, *24*, 155–170.
3. Ladam, G.; Schaaf, P.; Cuisinier, F. J. G.; Decher, G.; Voegel, J.-C. Protein Adsorption onto Auto-Assembled Polyelectrolyte Films. *Langmuir* **2001**, *17*, 878–882.
4. Lvov, Y.; Ariga, K.; Ichinose, I.; Kunitake, T. Assembly of Multicomponent Protein Films by Means of Electrostatic Layer-by-Layer Adsorption. *J. Am. Chem. Soc.* **1995**, *117*, 6117–6123.
5. Mertz, D.; Vogt, C.; Hemmerle, J.; Mutterer, J.; Ball, V.; Voegel, J. C.; Schaaf, P.; Lavalle, P. Mechanotransductive Surfaces for Reversible Biocatalysis Activation. *Nat. Mater.* **2009**, *8*, 731–735.
6. Mertz, D.; Vogt, C.; Hemmerle, J.; Debry, C.; Voegel, J.-C.; Schaaf, P.; Lavalle, P. Tailored Design of Mechanically Sensitive Biocatalytic Assemblies Based on Polyelectrolyte Multilayers. *J. Mater. Chem.* **2011**, *21*, 8324–8331.
7. Balabushevich, N. G.; Tiourina, O. P.; Volodkin, D. V.; Larionova, N. I.; Sukhorukov, G. B. Loading the Multilayer Dextran Sulfate/Protamine Microsized Capsules with Peroxidase. *Biomacromolecules* **2003**, *4*, 1191–1197.
8. Tiourina, O. P.; Sukhorukov, G. B. Multilayer Alginate/Protamine Microsized Capsules: Encapsulation of α-Chymotrypsin and Controlled Release Study. *Int. J. Pharm.* **2002**, *242*, 155–161.
9. Duan, L.; He, Q.; Wang, K. W.; Yan, X. H.; Cui, Y.; Möhwald, H.; Li, J. B. Adenosine Triphosphate Biosynthesis Catalyzed by F0F1 ATP Synthase Assembled in Polymer Microcapsules. *Angew. Chem., Int. Ed.* **2007**, *46*, 6996–7000.
10. Li, J.; Möhwald, H.; An, Z.; Lu, G. Molecular Assembly of Biomimetic Microcapsules. *Soft Matter* **2005**, *1*, 259–264.
11. Song, W.; He, Q.; Cui, Y.; Möhwald, H.; Diez, S.; Li, J. Assembled Capsules Transportation Driven by Motor Proteins. *Biochem. Biophys. Res. Commun.* **2009**, *379*, 175–178.
12. Shchepelina, O.; Drachuk, I.; Gupta, M. K.; Lin, J.; Tsukruk, V. V. Silk-on-Silk Layer-by-Layer Microcapsules. *Adv. Mater.* **2011**, *23*, 4655–4660.
13. Gazit, E. Self-Assembled Peptide Nanostructures: The Design of Molecular Building Blocks and Their Technological Utilization. *Chem. Soc. Rev.* **2007**, *36*, 1263–1269.
14. Knowles, T. P. J.; Oppenheim, T. W.; Buell, A. K.; Chirgadze, D. Y.; Welland, M. E. Nanostructured Films from Hierarchical Self-Assembly of Amyloidogenic Proteins. *Nat. Nanotechnol.* **2010**, *5*, 204–207.
15. Ulijn, R. V.; Smith, A. M. Designing Peptide-Based Nanomaterials. *Chem. Soc. Rev.* **2008**, *37*, 664–675.
16. Toksoz, S.; Guler, M. O. Self-Assembled Peptidic Nanostructures. *Nano Today* **2009**, *4*, 458–469.
17. Zhang, S.; Marini, D. M.; Hwang, W.; Santoso, S. Design of Nanostructured Biological Materials through Self-Assembly of Peptides and Proteins. *Curr. Opin. Chem. Biol.* **2002**, *6*, 865–871.
18. Duan, L.; He, Q.; Yan, X.; Cui, Y.; Wang, K.; Li, J. Hemoglobin Protein Hollow Shells Fabricated through Covalent Layer-by-Layer Technique. *Biochem. Biophys. Res. Commun.* **2007**, *354*, 357–362.
19. Qi, W.; Yan, X. H.; Juan, L.; Cui, Y.; Yang, Y.; Li, J. B. Glucose-Sensitive Microcapsules from Glutaraldehyde Cross-Linked Hemoglobin and Glucose Oxidase. *Biomacromolecules* **2009**, *10*, 1212–1216.
20. Tong, W.; Gao, C.; Möhwald, H. pH-Responsive Protein Microcapsules Fabricated *via* Glutaraldehyde Mediated Covalent Layer-by-Layer Assembly. *Colloid Polym. Sci.* **2008**, *286*, 1103–1109.
21. Furst, W.; Banerjee, A. Release of Glutaraldehyde from an Albumin–Glutaraldehyde Tissue Adhesive Causes Significant *in Vitro* and *in Vivo* Toxicity. *Ann. Thorac. Surg.* **2005**, *79*, 1522–1528.
22. Hennink, W. E.; van Nostrum, C. F. Novel Crosslinking Methods to Design Hydrogels. *Adv. Drug Delivery Rev.* **2002**, *54*, 13–36.
23. Berger, J.; Reist, M.; Mayer, J. M.; Felt, O.; Peppas, N. A.; Gurny, R. Structure and Interactions in Covalently and Ionically Crosslinked Chitosan Hydrogels for Biomedical Applications. *Eur. J. Pharm. Biopharm.* **2004**, *57*, 19–34.
24. Mart, R. J.; Osborne, R. D.; Stevens, M. M.; Ulijn, R. V. Peptide-Based Stimuli-Responsive Biomaterials. *Soft Matter* **2006**, *2*, 822–835.
25. Mi, L.; Fischer, S.; Chung, B.; Sundelacruz, S.; Harden, J. L. Self-Assembling Protein Hydrogels with Modular Integrin Binding Domains. *Biomacromolecules* **2005**, *7*, 38–47.
26. Wang, C.; Stewart, R. J.; KopeCek, J. Hybrid Hydrogels Assembled from Synthetic Polymers and Coiled-Coil Protein Domains. *Nature* **1999**, *397*, 417–420.
27. Westhaus, E.; Messersmith, P. B. Triggered Release of Calcium from Lipid Vesicles: A Bioinspired Strategy for Rapid Gelation of Polysaccharide and Protein Hydrogels. *Biomaterials* **2001**, *22*, 453–462.
28. Brandl, F.; Sommer, F.; Goepferich, A. Rational Design of Hydrogels for Tissue Engineering: Impact of Physical Factors on Cell Behavior. *Biomaterials* **2007**, *28*, 134–146.
29. Kim, B.; Lam, C. N.; Olsen, B. D. Nanopatterned Protein Films Directed by Ionic Complexation with Water-Soluble Diblock Copolymers. *Macromolecules* **2012**, *45*, 4572–4580.
30. Ji, J.; Li, B.; Zhong, W.-H. An Ultraelastic Poly(ethylene oxide)/Soy Protein Film with Fully Amorphous Structure. *Macromolecules* **2012**, *45*, 602–606.
31. Dierendonck, M.; De Koker, S.; De Rycke, R.; Bogaert, P.; Grooten, J.; Vervaet, C.; Remon, J. P.; De Geest, B. G. Single-Step Formation of Degradable Intracellular Biomolecule Microreactors. *ACS Nano* **2011**, *5*, 6886–6893.
32. Volodkin, D. V.; von Klitzing, R.; Möhwald, H. Pure Protein Microspheres by Calcium Carbonate Templating. *Angew. Chem., Int. Ed.* **2010**, *49*, 9258–9261.
33. Volodkin, D. V.; Schmidt, S.; Fernandes, P.; Larionova, N. I.; Sukhorukov, G. B.; Duschl, C.; Möhwald, H.; von Klitzing, R. One-Step Formulation of Protein Microparticles with Tailored Properties: Hard Templating at Soft Conditions. *Adv. Funct. Mater.* **2012**, *22*, 1914–1922.
34. Fasano, M.; Curry, S.; Terreno, E.; Galliano, M.; Fanali, G.; Narciso, P.; Notari, S.; Ascenzi, P. The Extraordinary Ligand Binding Properties of Human Serum Albumin. *IUBMB Life* **2005**, *57*, 787–796.
35. Varshney, A.; Sen, P.; Ahmad, E.; Rehan, M.; Subbarao, N.; Khan, R. H. Ligand Binding Strategies of Human Serum Albumin: How Can the Cargo be Utilized? *Chirality* **2010**, *22*, 77–87.
36. Petros, R. A.; DeSimone, J. M. Strategies in the Design of Nanoparticles for Therapeutic Applications. *Nat. Rev. Drug Discovery* **2010**, *9*, 615–627.
37. Kratz, F. Albumin as a Drug Carrier: Design of Prodrugs, Drug Conjugates and Nanoparticles. *J. Controlled Release* **2008**, *132*, 171–183.
38. Lu, G.; An, Z.; Tao, C.; Li, J. Microcapsule Assembly of Human Serum Albumin at the Liquid/Liquid Interface by the Pendent Drop Technique. *Langmuir* **2004**, *20*, 8401–8403.

39. An, Z.; Lu, G.; Möhwald, H.; Li, J. Self-Assembly of Human Serum Albumin (HSA) and L-α-Dimyristoylphosphatidic Acid (DMPA) Microcapsules for Controlled Drug Release. *Chem.—Eur. J.* **2004**, *10*, 5848–5852.
40. An, Z.; Tao, C.; Lu, G.; Möhwald, H.; Zheng, S.; Cui, Y.; Li, J. Fabrication and Characterization of Human Serum Albumin and L-α-Dimyristoylphosphatidic Acid Microcapsules Based on Template Technique. *Chem. Mater.* **2005**, *17*, 2514–2519.
41. An, Z.; Möhwald, H.; Li, J. pH Controlled Permeability of Lipid/Protein Biomimetic Microcapsules. *Biomacromolecules* **2006**, *7*, 580–585.
42. Mertz, D.; Tan, P.; Wang, Y.; Goh, T. K.; Blencowe, A.; Caruso, F. Bromoisobutyramide as an Intermolecular Surface Binder for the Preparation of Free-Standing Biopolymer Assemblies. *Adv. Mater.* **2011**, *23*, 5668–5673.
43. Auffinger, P.; Hays, F. A.; Westhof, E.; Ho, P. S. Halogen Bonds in Biological Molecules. *Proc. Nat. Acad. Sci. U.S.A.* **2004**, *101*, 16789–16794.
44. Metrangolo, P.; Resnati, G.; Pilati, T.; Liantonio, R.; Meyer, F. Engineering Functional Materials by Halogen Bonding. *J. Polym. Sci., Part A: Polym. Chem.* **2007**, *45*, 1–15.
45. Metrangolo, P.; Meyer, F.; Pilati, T.; Resnati, G.; Terraneo, G. Halogen Bonding in Supramolecular Chemistry. *Angew. Chem., Int. Ed.* **2008**, *47*, 6114–6127.
46. Metrangolo, P.; Resnati, G. Chemistry—Halogen *versus* Hydrogen. *Science* **2008**, *321*, 918–919.
47. Hardegger, L. A.; Kuhn, B.; Spinnler, B.; Anselm, L.; Ecabert, R.; Stihle, M.; Gsell, B.; Thoma, R.; Diez, J.; Benz, J.; *et al*. Systematic Investigation of Halogen Bonding in Protein−Ligand Interactions. *Angew. Chem., Int. Ed.* **2011**, *50*, 314–318.
48. Lu, Y.; Wang, Y.; Zhu, W. Nonbonding Interactions of Organic Halogens in Biological Systems: Implications for Drug Discovery and Biomolecular Design. *Phys. Chem. Chem. Phys.* **2011**, *12*, 4543–4551.
49. Parisini, E.; Metrangolo, P.; Pilati, T.; Resnati, G.; Terraneo, G. Halogen Bonding In Halocarbon−Protein Complexes: A Structural Survey. *Chem. Soc. Rev.* **2011**, *40*, 2267–2278.
50. Jiang, Y.; Alcaraz, A. A.; Chen, J. M.; Kobayashi, H.; Lu, Y. J.; Snyder, J. P. Diastereomers of Dibromo-7-epi-10-deacetylcephalomannine: Crowded and Cytotoxic Taxanes Exhibit Halogen Bonds. *J. Med. Chem.* **2006**, *49*, 1891–1899.
51. Becker, A. L.; Johnston, A. P. R.; Caruso, F. Layer-by-Layer-Assembled Capsules and Films for Therapeutic Delivery. *Small* **2010**, *6*, 1836–1852.
52. Rejman, J.; Oberle, V.; Zuhorn, I. S.; Hoekstra, D. Size-Dependent Internalization of Particles *via* the Pathways of Clathrin-and Caveolae-Mediated Endocytosis. *Biochem. J.* **2004**, *377*, 159–169.
53. Javier, M. A.; Kreft, O.; Semmling, M.; Kempter, S.; Skirtach, A. G.; Bruns, O. T.; del Pino, P.; Bedard, M. F.; Rädler, J.; Käs, J.; *et al*. Uptake of Colloidal Polyelectrolyte-Coated Particles and Polyelectrolyte Multilayer Capsules by Living Cells. *Adv. Mater.* **2008**, *20*, 4281–4287.
54. Yan, Y.; Johnston, A. P. R.; Dodds, S. J.; Kamphuis, M. M. J.; Ferguson, C.; Parton, R. G.; Nice, E. C.; Heath, J. K.; Caruso, F. Uptake and Intracellular Fate of Disulfide-Bonded Polymer Hydrogel Capsules for Doxorubicin Delivery to Colorectal Cancer Cells. *ACS Nano* **2010**, *4*, 2928–2936.
55. Elsner, N.; Dubreuil, F.; Weinkamer, R.; Wasicek, M.; Fischer, F. D.; Fery, A.; Grundke, K.; Stamm, M.; Adler, H.-J. Mechanical Properties of Freestanding Polyelectrolyte Capsules: A Quantitative Approach Based on Shell Theory. In *Characterization of Polymer Surfaces and Thin Films*; Grundke, K., Stamm, M., Adler, H.-J., Eds.; Springer: Berlin/Heidelberg, 2006; pp 117−123.
56. Fery, A.; Weinkamer, R. Mechanical Properties of Micro- and Nanocapsules: Single-Capsule Measurements. *Polymer* **2007**, *48*, 7221–7235.
57. Mosmann, T. Rapid Colorimetric Assay for Cellular Growth and Survival: Application to Proliferation and Cytotoxicity Assays. *J. Immunol. Methods* **1983**, *65*, 55–63.
58. Mecozzi, S.; West, A. P.; Dougherty, D. A. Cation-π Interactions in Aromatics of Biological and Medicinal Interest: Electrostatic Potential Surfaces as a Useful Qualitative Guide. *Proc. Nat. Acad. Sci. U.S.A.* **1996**, *93*, 10566–10571.